

# **Machine Learning assisted prediction of High Entropy Alloys Catalysts for Hydrogen Evolution Reaction.**

**M.Sc. Thesis**

By:

**BHAVYA JAIN**



**DEPARTMENT OF CHEMISTRY  
INDIAN INSTITUTE OF TECHNOLOGY INDORE  
JUNE 2021**



# Machine Learning assisted prediction of High Entropy Alloys catalysts for Hydrogen Evolution Reaction.

**A THESIS**

*Submitted in partial fulfilment of the  
requirements for the award of the degree  
of*

**Master of Science**

*by*

**BHAVYA JAIN**



**DEPARTMENT OF CHEMISTRY  
INDIAN INSTITUTE OF TECHNOLOGY INDORE**

**JUNE 2021**





# INDIAN INSTITUTE OF TECHNOLOGY INDORE

## CANDIDATE'S DECLARATION

I hereby certify that the work which is being presented in the thesis entitled **Machine Learning assisted prediction of High Entropy Alloy Catalysts for Hydrogen Evolution Reaction** in the partial fulfilment of the requirements for the award of the degree of **MASTER OF SCIENCE** and submitted in the **DEPARTMENT OF CHEMISTRY, Indian Institute of Technology Indore**, is an authentic record of my own work carried out during the time period from July 2020 to June 2021 under the supervision of **Dr Biswarup Pathak**, Associate Professor, Department of Chemistry, IIT Indore.

The matter presented in this thesis has not been submitted by me for the award of any other degree of this or any other institute.

**Signature of the student with date  
(Bhavya Jain)**

-----  
This is to certify that the above statement made by the candidate is correct to the best of my knowledge.

**Signature of the Supervisor of M.Sc. thesis with date  
(Dr Biswarup Pathak)**

-----  
**Bhavya Jain** has successfully given his MSc Oral Examination held on 08-06-2021,

Dr. Biswarup Pathak  
Signature of Supervisor of MSc thesis  
Date: 10-06-2021

Convener, DPGC  
Date:

Signature of PSPC Member  
Dr Dipak Kumar Roy  
Date: 10-06-2021

Signature of PSPC Member  
Dr Selvakumar Sermadurai  
Date: 10.06.2021



## Acknowledgements

With great pleasure, I want to express my deep sense of gratitude to my supervisor Dr. Biswarup Pathak (Associate Professor, Department of Chemistry, Indian Institute of Technology Indore) for providing me a wonderful opportunity to pursue research with his group and believing in my research abilities. His constant guidance, support, and motivation have been immensely helpful to complete this M.Sc. project. His enthusiasm and dedication have always inspired me. Further, I would like to thank my PSPC members Dr Dipak Kumar Roy and Dr Selvakumar Sermadurai for their valuable suggestions and support.

I wish to express my gratitude to the Director, IIT Indore for his continuous encouragement, help, and support in every aspect.

I am very grateful to Head, Department of Chemistry, Indian Institute of Technology Indore to constantly motivate me to research and providing us a nice environment. I am also grateful to Dr. Sampak Samanta, Dr. Chelvam Venkatesh, Dr. Anjan Chakraborty, Dr. Tridib Kumar Sarma, Dr. Suman Mukhopadhyay, Dr. Apurba Kumar Das, Dr. Rajneesh Misra, Dr. Sanjay Kumar Singh, Dr. Tushar Kanti Mukherjee, Dr. Satya S. Bulusu, Dr. Amrendra Kumar Singh, Dr. Abhinav Raghuvanshi, Dr. Dipak Kumar Roy, Dr. Selvakumar Sermadurai and Dr. Umesh A. Kshirsagar for their guidance and help during various activities.

I would like to extend my sincere thanks to my mentor Diptendu Roy for his kind and friendly nature and help in dealing with difficulties. I extend my deep thanks to my group members Dr. Preeti Bhauriyal, Dr. Gargee Bhattacharyya, Chiranjit Mondal, Sourabh Kumar, Akhil S. Nair, Shyama Charan Mandal, Rameshwar Lal Kumawat, Sandeep Das, Arunendu Das, Surya Sekhar Manna, Amitabha Das, Eti Mahal, Milan Kumar Jena and Nischal Bharadwaj, for their selfless co-operation and help to make my work successful.

I personally want to extend my thanks to my batch mates who were always there and never let me down during these M.Sc. days.

Most importantly none of this would have been possible without the support of my family and I deeply express my love and gratitude to my parents.

Finally, I would like to express my thanks to IIT Indore for the infrastructure, and all others who helped and supported me directly or indirectly.

**DEDICATED TO**

**MY FAMILY**

**AND ALL WELL-WISHERS...**



## Abstract

Innovation in the field of catalysis is of utmost importance to reduce reaction time and reaction efficiency. This requires sophistication in existing techniques and investigation of new, suitable materials for efficient catalytic design. Alloys as heterogeneous catalysts can be employed in comparison to pure elements. The Hydrogen Evolution Reaction (HER), a key step in the electrolysis of water, gives Hydrogen which can be considered as a very clean renewable energy resource compared to conventional fossil fuels. HER needs economic catalysts because of expensive pure element platinum electrocatalysts. In this study, we'll find out suitable High Entropy Alloys as the highly active catalysts for HER. To do so, we perform adsorption energy calculations for preparing training data from few selected surface microstructures using DFT with the PBE functional and GPAW. We wish to develop a simple model for the full distribution of adsorption energies involving random combinations of lattice positions using the prediction of a Machine Learning Algorithm. The optimization of the alloy then needs to be done so as to maximize catalytic activity using a suitable regression programming technique in the model algorithm. My aim is to engineer economically feasible catalysts for HER which in turn increases the prospects of Hydrogen as a clean renewable resource of energy.



# Table of Contents

	Page No.
<b>List of figures</b>	xv
<b>List of tables</b>	1
<b>Chapter-1: 1. Introduction</b>	<b>3-5</b>
<b>Chapter-2: 2. Computational Methods and Approximations</b>	
➤ <b>2.1. Schrödinger equation</b>	8
▪ <b>2.1.1. Schrödinger Equation for Multiple Body Systems</b>	8
▪ <b>2.1.2. The Born-Oppenheimer Approximation</b>	9
➤ <b>2.2. Hartree Fock Theory</b>	9
➤ <b>2.3. Density Functional Theory</b>	10
▪ <b>2.3.1. Hohenberg-Kohn Theorems</b>	10
▪ <b>2.3.2. Kohn-Sham Equations</b>	10-11
▪ <b>2.3.3. Exchange-correlation functional</b>	11
➤ <b>2.4. Projector Augmented Wave Method</b>	12-13
➤ <b>2.5. Computational Details</b>	14
<b>Chapter-3: Results, Discussion and Future Planning</b>	
➤ <b>3.1. Stability Analysis</b>	15-17
➤ <b>3.2. Hyperparameter Tuning</b>	18-21
➤ <b>3.3. Splitting of Train-Test Data</b>	22-24
➤ <b>3.4. Best Catalyst for HER</b>	25
<b>Chapter-5: Conclusion</b>	<b>26</b>
<b>6. References</b>	<b>27-31</b>



## List of Figures

### Page No.

<b>Figure 1:</b>	Plot for Omega vs. Delta (%) for all 500 combinations of 8-atom unit cells.	16
<b>Figure 2:</b>	Graph of Omega versus Delta% depicting stable solid solution formation only.	17
<b>Figure 3:</b>	Surface Microstructure illustration for hcp-hollow site adsorption.	19
<b>Figure 4:</b>	Surface Microstructure with the input features. There are 15 parameters for adsorption in hcp-hollow site. The colours differentiate the metal atoms. Green: Ni, Pink: Co, Brown: Cu, Reddish brown: Fe, Blue: Zn.	21
<b>Figure 5:</b>	A sample plot of Cross Linear Regression showing predicted value versus observed value. The difference between the predicted value and the observed (calculated value) will provide us the mean absolute error.	23
<b>Figure 6:</b>	The outline and the future planning of the work summarized in a flowchart. The main focus is to explore the HEA CuCoNiZnFe for Hydrogen Evolution Reaction so that hydrogen can be used as a clean renewable resource of energy.	24



## List of Tables

Page No.

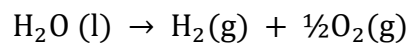
<b>Table 1:</b>	The encoding is done such that 1 is at that position which signifies the adsorbing site for the microstructure. For the surface and subsurface nearest neighbour region, the number of atoms becomes the parameter.	20
-----------------	---	----



## **CHAPTER 1: INTRODUCTION**

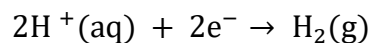
Approximately 80% of the global energy demand is satisfied by the non-renewable resources of energy and only 20% by the renewable, alternative energy resources. Ever increasing demand and reducing availability of non-renewable, conventional sources of energy has led to the active research for alternative sources of energy since the last century. In this context, hydrogen as an alternative clean fuel source has remarkable potential which can be utilized to meet this enormous energy demand.

However, there are considerable obstacles to fully tap and utilize this resource.<sup>1</sup> The Hydrogen Evolution Reaction (HER) leads to the hydrogen gas production from the electrochemical splitting, or electrolysis of water. The electrolysis of water is given by the reaction below:

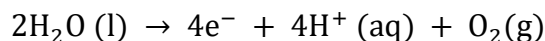


$\Delta G^\circ = +237.2 \text{ kJ mol}^{-1}$ ,  $\Delta E^\circ = 1.23 \text{ V}$  vs standard hydrogen electrode (NHE) involves two half-cell reactions:

1. The Hydrogen Evolution Reaction (HER)

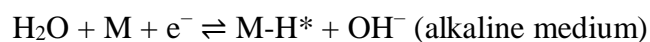


2. The Oxygen Evolution Reaction (OER)

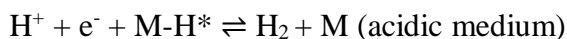


The Hydrogen adsorption reaction can be described by the Volmer mechanism. The Tafel mechanism and Heyrovsky mechanism shows the desorption of the adsorbate from the catalyst.<sup>2</sup>

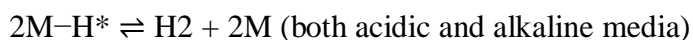
- 1) Hydrogen adsorption (described by Volmer mechanism)



(2) Hydrogen desorption (described by Heyrovsky mechanism)



(3) Hydrogen desorption (as per Tafel Mechanism)



There is an inherent barrier observed experimentally for the evolution of  $\text{H}_2$  and  $\text{O}_2$  gases in HER and OER which is known as Overpotential ( $\eta$ ). Overpotential is the excess potential between the experimental value and the thermodynamic value of potential required to carry out the electrolysis which is usually lost as heat. Minimization of overpotentials of the HER and the OER require the presence of catalysts.<sup>4</sup>

HER involves the usage of catalysts involving noble metals such as platinum, palladium, rhodium and so on which are quite expensive. Platinum based catalysts are currently most effective because of their optimum Gibbs Free Energy for hydrogen adsorption ( $\Delta G_{\text{H}^*}$ ) and high exchange current density ( $j_0$ ). They also provide low activation energy pathway for hydrogen desorption.

However, low abundance and really high cost of Platinum hinder the practical applications of hydrogen as a fuel. Nevertheless, there is considerable investigation for reducing and even replacing noble metals for this purpose. The avant-garde advances and research in this field is quite active for the development of low cost and high efficiency catalysts.<sup>5</sup>

Heterogeneous catalysts are easy to work with, avoiding the formation of inorganic salts. They can be recycled or reused and their storage and disposal is relatively easier than homogeneous catalysts. The separation of homogeneous catalysts from the reaction mixture is quite tedious and expensive requiring extraction or distillation.<sup>6</sup>

Heterogeneous catalysts, being different phase, are very easy to remove from the reaction mixture. They remain robust at extreme conditions of temperature and pressure. Due to these advantages, the chemical processes can be streamlined according to our needs, while operational cost remains low.

Innovation in the field of catalysis is of utmost importance to reduce reaction time and reaction efficiency. This requires sophistication in existing techniques and investigation of new, suitable materials for efficient catalytic design. Alloys as heterogeneous catalysts can be employed in comparison to pure elements.<sup>7</sup>

High Entropy Alloys (HEAs) are formed by mixing equal or relatively large proportions of (usually) five or more elements. The term is coined as “High Entropy” because mixing more elements in similar proportions increase entropy of mixing.

In our study, constituent elements are chosen with similar atomic radii are likely to form a stable HEA. HEAs form a defined crystal with constituent elements in random order. Their surfaces can provide atomic combinations with high catalytic activity.

The surface possibilities in HEAs inspire the investigation of HEA for their usage as a catalyst. Owing to the large number of particular combinations giving distinctive environment for each combination, catalytic surface of HEA can provide a continuum of adsorption energies with very little energy gap and the sites with optimal characteristics control the catalytic activity. Hence, tuning of composition of HEA surface can be performed which could lead to the highest possible activity.<sup>8</sup>

The interaction between catalyst and intermediates plays a very important role in choosing constituents for HEAs, in accordance with Sabatier Principle. Volcano plots show that Gibbs free energy of hydrogen adsorption should be close to zero with high exchange current density for exemplary activity.

Large positive Gibbs free energy shows quite weak hydrogen attachment to the catalyst, whereas high magnitude of negative Gibbs free energy shows very strong hydrogen attachment to the catalyst leading to weak desorption.

Platinum, palladium, and rhodium though exhibit excellent properties for HER, but because of the rarity of the noble metal reserves, are quite costly for practical applications. Amongst the earth abundant metals, Nickel stands out as the strongest candidate for HER, since it possesses the most ideal characteristics of minimum  $\Delta G_{H^*}$  and high  $j_0$  and Cobalt comes as a close second. Iron, Zinc and Copper have been chosen as constituents of HEAs since they have been previously used in combination with noble metal as catalysts to reduce the latter percentage.<sup>9</sup>

Higher numbers of surface arrangements on HEA catalyst, make it unfeasible to carry out quantum mechanical simulations on each arrangement. The solution to this problem is employing Machine Learning for predicting catalytic activity of a large number of sites by using a training data set, so that the HEAs can be tailored with suitable sites possessing optimum activity properties.

## CHAPTER 2: COMPUTATIONAL METHODS AND APPROXIMATIONS

### 2.1. Schrödinger Equation

The Schrödinger equation is the fundamental equation of quantum mechanics. The solution of the Schrödinger wave equation gives us the wave function of the electron. It is a partial wave function which uses the concept of conservation of energy to obtain information about the electron. It is given by the following equation 2.1:

$$\hat{H}\Psi(x) = E\Psi(x) \quad (2.1)$$

where  $\hat{H}\Psi(x)$  is the Hamiltonian operator and given by,

$$\hat{H} = \frac{-\hbar^2}{2m} \frac{\partial^2}{\partial x^2} + V(x) \quad (2.2)$$

and  $E\Psi(x)$  is the total energy.<sup>[3]</sup>

While, time dependent Schrödinger equation is given as,

$$\hat{H}\psi = i\hbar \frac{d\psi}{dt} \quad (2.3)$$

Here,  $\hbar$  is given by  $\frac{h}{2\pi}$ , and  $h$  is Planck's constant. This time dependent Schrödinger equation is the basis of most of the quantum chemical calculations.

However, the given equation 2.2 can be easily solved for single electron system (like H, He<sup>+</sup>, Li<sup>2+</sup> etc.) but the solvation of the expression 2.2 is difficult for a many electrons system.<sup>10</sup>

### 2.1.1 Schrödinger Equation for Multiple Body Systems

Solving the Schrödinger equation for a multi-electron system is a bit of hassle as in multi-electron system the exact equation cannot be separated into the uncoupled equation.

The Schrödinger equation for many electron systems is given as:

$$\hat{H} \Psi(x_1, x_2, \dots, x_n, r_1, r_2, \dots, r_n) = E \Psi(x_1, x_2, \dots, x_n, r_1, r_2, \dots, r_n) \quad (2.4)$$

In the equation 2.3,  $x_1, x_2, \dots, x_n$  represent position coordinates of electrons and  $r_1, r_2, \dots, r_n$  represent position coordinates of the nucleus.<sup>11</sup>

For many electron systems the Hamiltonian operator is given as follows

$$H = T_e + T_n + V_{ee} + V_{nm} + V_{ne} \quad (2.5)$$

Where  $T_e, T_n$  represents the total energy due to the motion of the electrons and nucleus, respectively, while  $V_{ee}, V_{nm}$  represents the coulombic interaction between electrons and nuclei, respectively,  $V_{ne}$  corresponds to the coulombic interactions between nucleus and electron. Hence, the extended Hamiltonian operator is given by equation 2.6.

$$H_{tot} = \sum \frac{p_i^2}{2m} + \sum \frac{p_I^2}{2M_I} + \sum V_{nucl}(r_i) + \frac{1}{2} \sum_{i \neq j} \frac{e^2}{|r_i - r_j|} + \frac{1}{2} \sum_{I \neq J} \frac{z_I z_J e^2}{|R_I - R_J|} \quad (2.6)$$

Here in equation 2.6,  $V_{nuc}(r) = -\sum_I \frac{z_I e^2}{|r - R_I|}$  (2.6.1)

For solving this equation, some approximations are used which permits us to separate the function into the uncoupled equation. Three major approximations are: (1) The Born-Oppenheimer approximation, (2) The independent particle approximation, and (3) The  $\pi$ -electron separation approximation. Below we have discussed the Born-Oppenheimer approximation.<sup>12</sup>

### 2.1.2. The Born-Oppenheimer Approximation

The Born-Oppenheimer approximation states that the nuclei is heavy and slow whereas electrons are also small but fast (can respond almost instantaneously to any change in the nuclear coordinates), which means we can decouple the dynamic of the nuclei and the electrons. In this approximation, the nuclear kinetic energy term can be neglected and the nuclear-nuclear repulsion term can be taken as a constant.<sup>13</sup>

Hence, the Hamiltonian operator becomes:

$$H_{tot} = \sum \frac{p_i^2}{2m} + \frac{1}{2} \sum_{i \neq j} \frac{e^2}{|r_i - r_j|} + \frac{1}{2} \sum_{I \neq J} \frac{z_I z_J e^2}{|R_I - R_J|} \quad (2.7)$$

Even after the application of BO approximation, the solution for the many-electron systems wave function is computationally too expensive. Keeping this in view, other approximations like density functional theory (DFT) are very beneficial.

### 2.2. Hartree Fock Theory

Hartree Fock theory is used for the approximation of multiple bodies of wavefunctions. A single Slater determinant of  $N$  spin-orbitals will furnish the wavefunction in this approximation.

$$\Psi = \begin{vmatrix} \psi_1(\mathbf{x}_1) & \psi_1(\mathbf{x}_2) & \dots & \psi_1(\mathbf{x}_N) \\ \psi_2(\mathbf{x}_1) & \psi_2(\mathbf{x}_2) & \dots & \psi_2(\mathbf{x}_N) \\ \dots & \dots & \dots & \dots \\ \psi_N(\mathbf{x}_1) & \psi_N(\mathbf{x}_2) & \dots & \psi_N(\mathbf{x}_N) \end{vmatrix} \quad (2.8)$$

Here the coordinates in space are given by variables  $\mathbf{x}$ . This wavefunction obtained is antisymmetric i.e., the sign will change upon the interchange of any two electron positions in accordance with Pauli Exclusion Principle.<sup>14</sup>

$$\Psi(\mathbf{x}_1, \mathbf{x}_2, \dots, \mathbf{x}_i, \dots, \mathbf{x}_j, \dots, \mathbf{x}_N) = -\Psi(\mathbf{x}_1, \mathbf{x}_2, \dots, \mathbf{x}_j, \dots, \mathbf{x}_i, \dots, \mathbf{x}_N) \quad (2.9)$$

This theory assumes neglect of the interelectronic correlation by taking a single determinant for the wavefunction. There is an average potential assumed from the other electrons which is a huge approximation and not very precise.<sup>15</sup>

### 2.3. Density Functional Theory

DFT is a computational quantum mechanical modelling method used in Physics, Chemistry, and Material Science to investigate the electronic structure (ground state) of many-body systems. Using this theory, the properties of a many-electron system can be determined by using Functionals. In DFT, instead of considering wave function, we considered density functional.<sup>16</sup>

DFT: work in terms of density

$$E = E[\eta(r)] \quad (2.10)$$

$$\varphi^2 = \eta(r) \quad (2.11)$$

#### 2.3.1. The Hohenberg and Kohn (HK) theorem

HK theorem is known as the heart of DFT. It proposes the following things:

1. Every observable such as ground state energy is a unique function of the ground state density.
2. The electron density which minimizes the energy of the overall function is the true ground state energy.

The HK theorem provides a method for minimizing energy by changing electron density but it is not capable of providing the relation between kinetic energy and density.<sup>17</sup>

#### 2.3.2. Kohn Sham Equations

To understand the electron density functions clearly, Kohn and Sham have proposed a set of equations. For this the many-body system is replaced by a fictitious system of non-interacting electrons. They fractionized the total energy functional into the different parts as described in equation 2.7.

$$E[\rho(r)] = T_0[\rho(r)] + \frac{1}{2} \iint \frac{\rho(r)\rho(r')}{|r-r'|} dr dr' + \int V_{ext}(r)\rho(r)dr + E_{xc}[\rho(r)] + E_{II} \quad (2.12)$$

In the above equation 2.12,  $T_0[\rho(r)]$  represents the energy due to the motion of the electrons in a system having electron density  $\rho$  same as that of real system excluding electron-electron interactions.<sup>18</sup>

Second term in the equation 2.12,  $\frac{1}{2} \iint \frac{\rho(r)\rho(r')}{|r-r'|} dr dr'$  represents the pure coulombic interaction between the electrons, third term  $\int V_{ext}(r)\rho(r)dr$  is the interaction between core and valence electrons. The fourth term  $E_{xc}[\rho(r)]$  is known as exchange-correlation energy which takes care of all the quantum interactions between electrons needed to be approximated. The last term  $E_{II}$  represents the nuclei-nuclei interactions. However, the above equation can be reduced in the following form

$$E[\{\Psi\}] = E_{known}[\{\Psi\}] + E_{xc}[\{\Psi\}] \quad (2.13)$$

Where,  $E_{known}$  is sum of the all the known parameters such as kinetic energy, potential energy and all the coulombic interactions which can be easily obtained. While,  $E_{xc}$  can only be solved by knowing the value of exchange-correlation potential. However, getting these values is very difficult.<sup>19</sup>

### 2.3.3. Exchange-correlation functional

In equation (2.8), the unknown parameter is an exchange correlation functional, which is generally approximated by the Kohn-Sham equation.  $E_{xc}$  can be expressed as a sum of electron exchange and electron correlation as described as follows.

$$E_{xc} = E_x + E_c \quad (2.14)$$

Various local functional are used for approximating the exchange correlational energy such as Projector Augmented Wave Method.<sup>20</sup>

## 2.4. Projector Augmented Wave Method (PAW)

Since the electronic wave functions of true materials have different behaviour in different regions. i.e., in bonding (or valence region) the oscillation of wave function is very smooth while for the electrons in cores the oscillation is very rapid. In general valence electrons are described by a plane wave basis set while, Core electrons could not be represented by the plane wave basis set due to their high computational cost. Hence this method uses the partial wave function to represents the electron in the augmented region. In PAW method, the highly oscillating wave function transforms to smoother form which depends on the linear transformation operator (T). The linear transformation operator transforms a wavefunction into pseudo wave function.

$$|\Psi_n\rangle = T|\psi_n\rangle \quad (2.15)$$

Where  $\Psi_n$  represents the pseudo wave function. The wave functions ( $|\psi_n\rangle$  and  $|\Psi_n\rangle$ ) are expressed as a linear combination of partial waves for each augmentation regions as described below:

$$|\psi_n\rangle = \sum_i c_i |\phi_i\rangle \quad (2.16)$$

$$|\Psi_n\rangle = \sum_i c_i |\tilde{\phi}_i\rangle \quad (2.17)$$

The operator T is given by

$$T = 1 + \sum_i (|\phi_n\rangle - |\tilde{\phi}_n\rangle) \langle \tilde{p}_i | \quad (2.18)$$

Where,  $\langle \tilde{p}_i |$  is the projection function which is initiated from different practical schemes. In this context, pseudopotential helps to get rid from the problem of core and valence electrons. There are a variety of pseudopotentials which can transfer oscillating wave function to a smoother one. However, the PAW is combined with the ultra-soft pseudopotentials and augmented-planewave.<sup>21</sup>

## **GPAW**

GPAW is a density-functional theory (DFT) Python code based on the projector-augmented wave (PAW) method and the atomic simulation environment (ASE). It uses plane-waves, atom-centric basis-functions or real-space uniform grids combined with multigrid methods.

## 2.5. Computational Details

PBE functional using the Atomic Simulation Environment (ASE) and the GPAW code were used for performing DFT calculations using a plane-wave expansion of the wavefunction.<sup>22</sup>

Planar  $3 \times 4 \times 4$  atoms slabs with a plane-wave cut-off at 400 eV were used to calculate adsorption energies. Monkhorst-Pack k-point sampling of the Brillouin zone of (4,4,1) was used for the CuCoNiZnFe high entropy alloy. The slabs were relaxed to a maximum force criterion of 0.09 eV/Å on the atoms. The top and bottom of the slabs were subjected to a vacuum of 10 Å. The positions of the atoms were fixed for all while the two top layers were allowed to relax. The adsorption energies of molecules O and H were calculated employing identical super cells. The same DFT calculations and features were used as for the slabs. The adsorption energies of O and H were calculated as:

$$\Delta E_O = E_{O^*} - E_* - \frac{1}{2}E_{O_2} \quad (2.19)$$

$$\Delta E_H = E_{H^*} - E_* - \frac{1}{2}E_{H_2} \quad (2.20)$$

where  $\Delta E_H$  and  $\Delta E_O$  are the adsorption energies of H and O respectively.  $E_{H^*}$  and  $E_{O^*}$  are the density functional theory calculated energies of the relaxed slabs when the adsorbate is present.  $E_*$  is the density functional theory energy of the slab when the adsorbate is not present.  $E_{H_2}$  and  $E_{O_2}$  are the DFT energies of the molecular gases.<sup>23</sup>

The lattice parameter for the slabs was chosen as the weighted average of the DFT-calculated lattice parameters of the constituent elements in the top layer of the slab. The lattice parameter is expected to take consideration of the effect of strain in HEA surface in real cases.<sup>24</sup>

The lattice parameters corresponding to a minimum in energy of the individual elements were also calculated. A primitive fcc unit cell was used for this purpose. The lattice parameter of Ni was found to be 3.499 Å.

## **CHAPTER 3: RESULTS, DISCUSSION AND FUTURE PLANNING**

### **3.1. Stability Analysis**

The stability of a High Entropy Alloy owes to its remarkably large degree of randomness which leads to high entropy which in turn minimizes free energy. The study of stability required the parameters of atomic radii and composition of the metal constituents in the alloys.

Theoretical stability of the HEA is verified by performing stability analysis by checking the parameters of the atomic radius difference factor ( $\delta$ ) and ratio of entropy of mixing and enthalpy of mixing ( $\Omega$ ).<sup>31</sup>

Optimizing the configuration or the framework of the alloy leads to the design of a potential suitable HEA and the discovery pathway for new alloys.

The stability is put to test by taking a unit cell of 8 atoms and the lattice points were assigned atoms randomly. The lattice parameter of the unit cell was found by taking the weighted average of the pure bulk parameters.

500 unit-cells were taken and  $\delta$  and  $\Omega$  values were found for each cell.

From previous reports, it is observed that the  $\delta$  and  $\Omega$  values must be smaller than 6.6% and larger than 1.1% respectively.<sup>32</sup>

Following these values, the formation of a stable solid solution is possible. The stability analysis of 500 combinations was done using the parameters of omega and delta%.

Figure 1 shows the plot of omega and delta% for the 500 combinations and Figure 2 shows the plot for the combinations exhibiting stable solid solution formation only with  $\delta < 6.6\%$  and  $\Omega > 1.1$ .

## Discussion on $\delta$ and $\Omega$

### 1. Delta ( $\delta$ )

The equation for the atomic radius difference factor is given as:

$$\delta = \sqrt{\sum_{i=1}^N c_i (1 - r_i/r_{avg})^2} \quad (3.1)$$

Here,  $c_i$  is the percentage composition of metals in unit cells,  $r_i$  is the radius of individual component,  $r_{avg}$  is the average radius and N is the number of constituent metals.<sup>33</sup>

### 2. Omega ( $\Omega$ )

Omega is the ratio taken of the product of average melting temperature of the constituents and entropy of mixing and the enthalpy of mixing.

$$\Omega = \frac{T_m \Delta S_m}{|\Delta H_m|} \quad (3.2)$$

Entropy of mixing is given by

$$\Delta S_m = -R \sum_{i=1}^N c_i \ln c_i \quad (3.3)$$

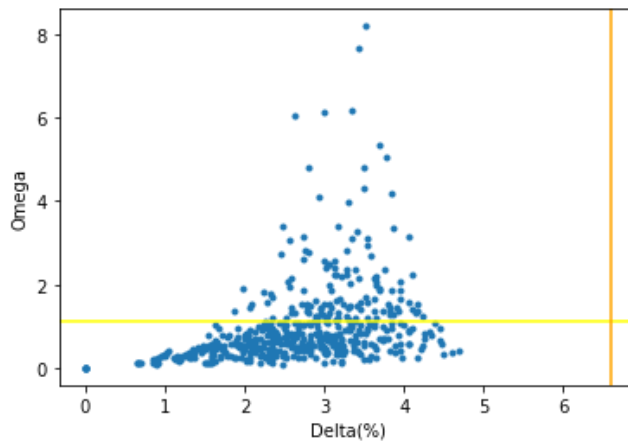


**Figure 1:** Plot for Omega vs. Delta (%) for all 500 combinations of 8-atom unit cells.

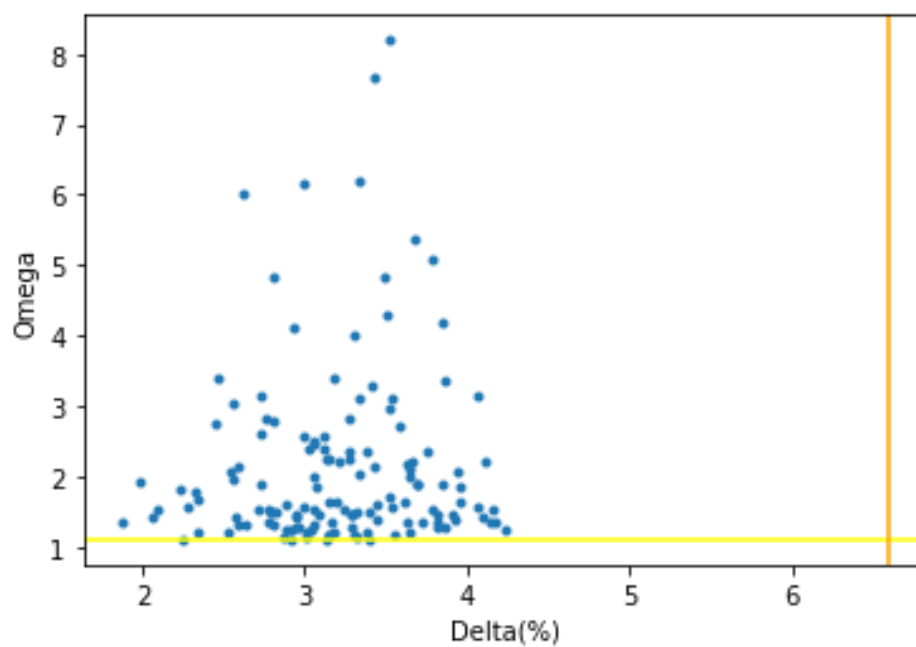


**Figure 2:** Plot for Omega versus Delta% depicting stable solid solution formation only.

Out of 500 combinations of 8-atom unit cells, 137 unit-cells have been found in the necessary bounded region of the parameters. These stable unit cells have been used for constructing the required supercells for finding catalysts.

### 3.2. Hyperparameter Tuning

A hyperparameter is an argument of the model whose value is set before the machine learning process is set. The tuning of hyperparameters has to be done so that the optimum hyperparameters can be chosen for a machine learning algorithm.<sup>34</sup>

#### Hyperparameter types:

- K in K-NN
- Regularization constant, kernel type, and constants in SVMs
- Number of layers, number of units per layer, regularization in neural network

#### Generalization (test) error of learning algorithms has two main components:

- Bias: error due to simplifying model assumptions
- Variance: error due to randomness of the training set

The trade-off between these components is determined by the complexity of the model and the amount of training data. The optimal hyperparameters help to avoid under-fitting (training and test error are both high) and over-fitting (Training error is low but test error is high).

HEAs provide a very high number of surface microstructures which leads to the optimization of the catalytic properties such as the required optimum values of the H adsorption energies and O adsorption energies.

The huge number of microstructures leads to the correspondingly large number of adsorption energies which is impossible to calculate using ab initio method. The solution is to take a simple model employing a small set of DFT calculated adsorption energies for the commensurate microstructures as the input for the machine learning algorithm.

There are many algorithms available for Supervised Machine learning. The Gaussian process regression is generally found to give small errors in prediction of adsorption energies.

It permits for the evaluation of adsorption in a nonlinear fashion which is done by giving weightage to the microstructures in the training set more similar to the surface being checked. The GPR algorithm requires kernel and tuned hyperparameters and can be implemented in the open source scikit-learn.<sup>35</sup>

The type of adsorption can be on-top adsorption and hollow site adsorption. The three metal atoms forming a hollow site can have 35 possibilities if we consider the combinations with replacement of 5 elements. The formula for combinations with replacements is:

$$C^R(n, r) = \frac{(n + r - 1)!}{r! (n - 1)!} \quad (3.4)$$

Also, the labelling of regions is done for the two nearest neighbour or coordination spheres. Figure 3 shows the hcp-hollow adsorption with the white circle being the hydrogen atom. The adsorption of H and O in a hollow site are considered for hcp-hollow site and fcc-hollow sites for this work.

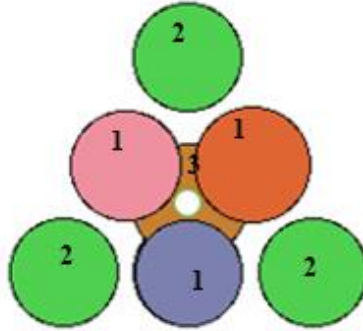


**Figure 3:** Surface Microstructure illustration for hcp-hollow site adsorption. The labelled areas 1, 2 and 3 are the adsorbing sites, surface nearest neighbour subsurface nearest neighbour regions respectively. The white circle represents the hydrogen atom adsorbed in the adsorbing site.

The possibilities of the 5 elements in the adsorbing site and the first and second nearest neighbour regions lead to the total of  $35 \times 35 \times 35 = 42,875$  and  $35 \times 35 \times 5 = 6125$  distinct microstructures for fcc-hollow and hcp-hollow adsorption. The input features can be found from the microstructure itself.

The input features are followed from the publication for which the reference is given.<sup>36</sup> The total of the number of atoms in the adsorbing site region and in the first and second nearest neighbour regions become the parameters for input features.

There are 15 parameters for hcp-hollow, together with the labelling of the elements in the adsorbing site and the two nearest surface and subsurface coordination regions.

The input features also include the adsorption energy which is found via density functional theory calculations for a particular surface microstructure.

Figure 4 illustrates one of the surface microstructures and Table 1 the corresponding input description for the hcp-hollow adsorbing site.

0	1	0	1	1
Cu	Co	Ni	Zn	Fe

a)

0	0	3	0	0
Cu	Co	Ni	Zn	Fe

b)

1	0	0	0	0
Cu	Co	Ni	Zn	Fe

c)

**Table 1:** The encoding is done for a) the adsorbing site, b) the nearest region of adsorption site and c) subsurface nearest neighbour region for the given microstructure in Figure 4.

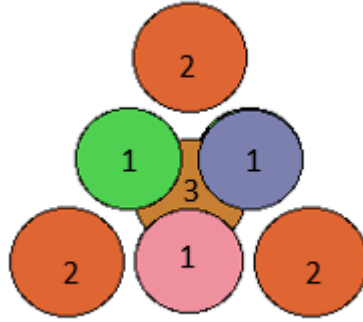


**Figure 4:** Surface Microstructure with the input features. There are 15 parameters for adsorption in hcp-hollow site. The colours differentiate the metal atoms. Green: Ni, Pink: Co, Brown: Cu, Reddish brown: Fe, Blue: Zn.

**Optimal Hyperparameters:** Hyperparameters control the over-fitting and under-fitting of the model. Optimal hyperparameters often differ for different datasets. To get the best hyperparameters the following steps are followed:

1. For each proposed hyperparameter setting the model is evaluated
2. The hyperparameters that give the best model are selected.

**Hyperparameters Search:** Grid search picks out a grid of hyperparameter values and evaluates all of them. Guesswork is necessary to specify the min and max values for each hyperparameter. Random search randomly values a random sample of points on the grid. It is more efficient than grid search. Smart hyperparameter tuning picks a few hyperparameter settings, evaluates the validation matrices, adjusts the hyperparameters, and re-evaluates the validation matrices. Examples of smart hyper-parameter are Spearmin (hyperparameter optimization using Gaussian processes).<sup>37</sup>

In this process, tuning for Hyperparameters can be performed for the applied machine learning algorithms.

### 4.3. Splitting of Train-Test Data

The Gaussian Process Regression (GPR) algorithm is provided with 80% of the microstructures which are grouped in the Training Data set with the corresponding adsorption energies H and O adsorbed in hcp -hollow site calculated with the help of DFT.

The remaining 20% of the microstructures are grouped into the Test Data set. They are used for predicting or evaluating the performance of a statistical model which can be done using 5-fold cross validation.<sup>38</sup> This is called as the Splitting of Train-Test Data.

On similar grounds using Splitting of Train-Test Data, we can be able to get the distribution of predicted adsorption energies via machine learning for all the possible surface microstructures of CuCoNiZnFe HEA.

In the hcp-hollow and fcc-hollow site cases, there are total 6125 distinct and 42,875 distinct microstructures respectively.

The favourable adsorption sites for hydrogen adsorption are fcc-hollow sites and hcp-hollow sites. We have planned to take around 1% data from whole data set as training data which is around 61 and 420 adsorption energies for hcp-hollow and fcc-hollow sites respectively. Due to the time constraint, we're able to find the training data set consisting of 29 microstructures for hcp-hollow site. In the future, we wish to find the training data set for fcc-hollow site as well.

This training data set data set has been planned to use for the prediction of adsorption energies using a suitable Machine Learning algorithm. A plot of Machine Learning algorithm predicted adsorption energies versus DFT-calculated adsorption energies can then be plotted where  $\Delta E_{\text{pred}} - \Delta E_{\text{DFT}}$  will provide us the mean absolute error. Figure 5 shows a sample cross linear regression plot which employs the method of least squares in linear regression analysis.

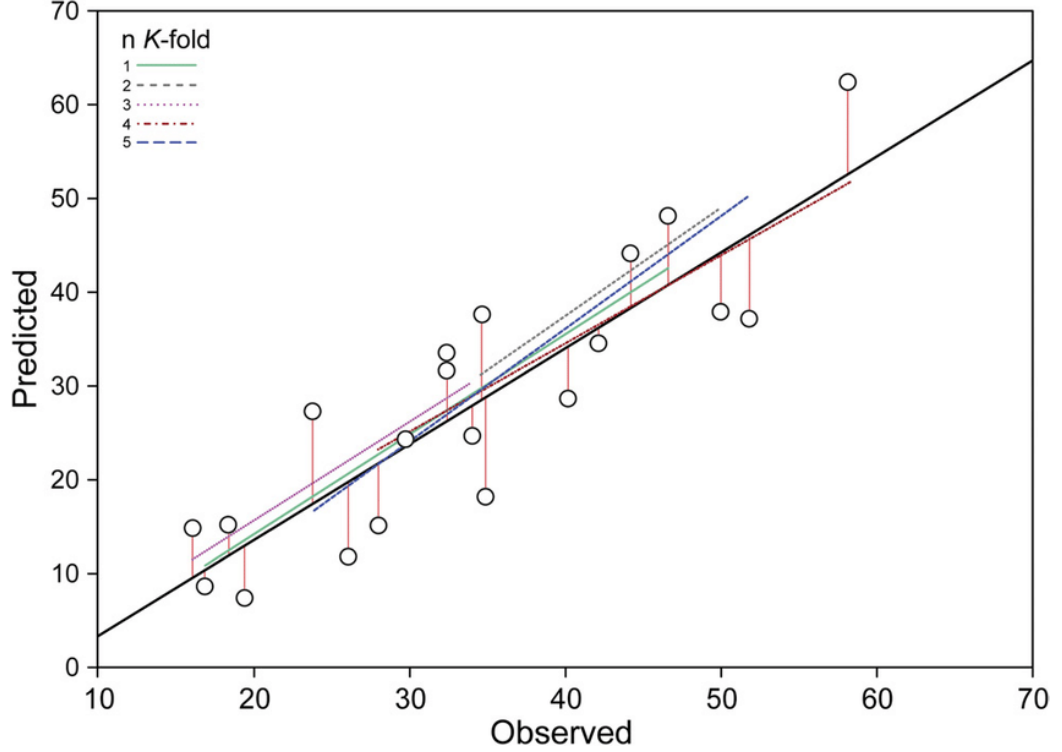


**Figure 5:** A sample plot of Cross Linear Regression showing predicted value versus observed value. The difference between the predicted value and the observed (calculated value) will provide us the mean absolute error.

The predicted adsorption energies can then be employed for the optimization of catalytic activity as discussed in the next section.

The contribution of a surface microstructure or the probability is dependent on the composition of the HEA. It is given as:

$$P_i(\mathbf{f}) = \prod_{k=1}^M f_k^{n_{ik}} \quad (3.5)$$

In this equation,  $P_i(\mathbf{f})$  is given as the probability of the microstructure  $i$ ,  $\mathbf{f}$  is a vector formed from molar fractions,  $M$  is the total elements which constitute the HEA,  $f_k$  is the molar fraction, and  $n_{ik}$  is the number of atoms where  $k$  is the element. The probability found for each microstructure can then be utilized to optimize the catalytic activity as found in the next section.

## FLOWCHART

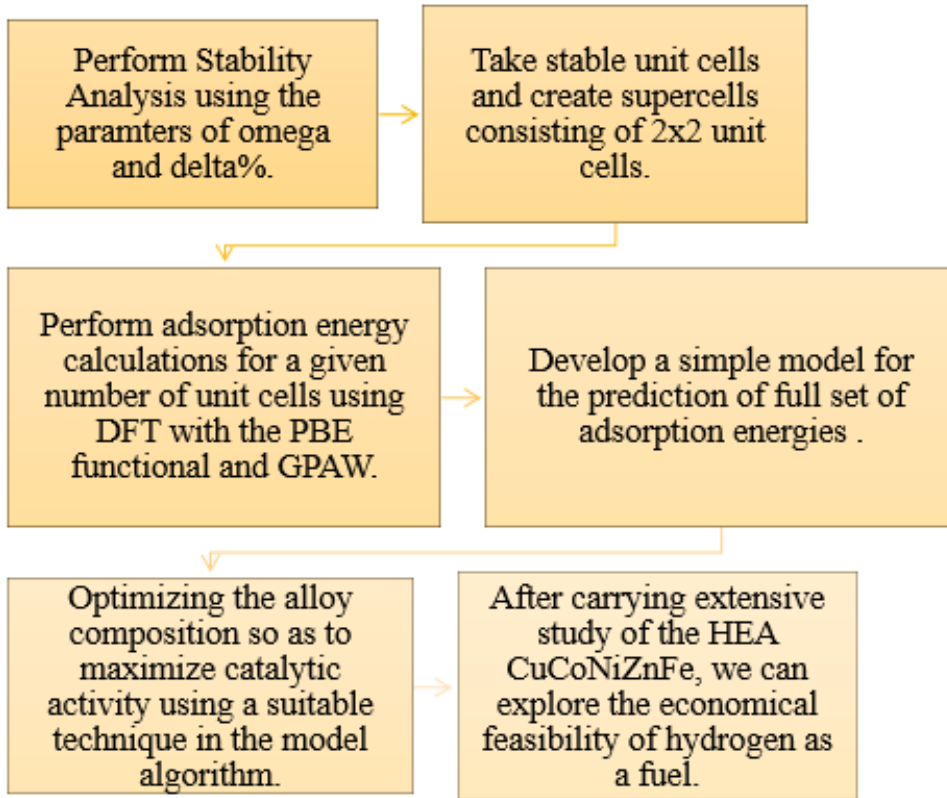


**Figure 6:** The outline for future planning of the work to explore the HEA CuCoNiZnFe as catalyst for Hydrogen Evolution Reaction.

#### 4.4. Best Catalyst for HER

The best fit for the catalyst for Hydrogen Evolution Reaction is found by optimization of the alloy constituents. The refinement of surface is performed after covering the whole range of distributions. The optimum binding energy is linked to finding particular sites. Based on the Sabatier principle, we can quantify the catalytic activity  $A$  in equation 4.6 as follows:

$$A = \sum_{i=1}^Z \left( \prod_k^{metals} f_k^{n_{ik}} \right) \exp \left( -\frac{|\Delta E_i - \Delta E_{opt}|}{k_B T} \right) \quad (3.6)$$

Here,  $Z$  is the number of surface configurations,  $f_k$  is the atomic fraction,  $n_{ik}$  is the number of element  $k$  in configuration 'i',  $\Delta E_i$  is the adsorption energy found from the model, and  $\Delta E_{opt}$  is the optimum energy according to the Sabatier principle.<sup>5</sup>

A non-linear enhancement method, called sequential least squares programming (SLSQP) can be used for the algorithm to find the maximum of the activity.

The random configuration takes account of the possibility of each site. Each site probability is considered along with the difference of the site energy and the optimum energy. The summation of all the contributions provides us the relation of the catalytic activity.<sup>39</sup>

Pure Pt provides Gibbs free adsorption energy of the magnitude near to zero eV to \*H intermediate which is quite optimum. Thus, it is quite advantageous to find a catalyst having characteristics mirroring that of pure Platinum.

The mixture  $\text{Cu}_{20}\text{Co}_{20}\text{Ni}_{20}\text{Zn}_{20}\text{Fe}_{20}$  can be taken which is then optimized using the SLSQP algorithm or any other suitable algorithm to find the high entropy alloy possessing the maximum of catalytic activity and the minimum of overpotential. Reduction in overpotential from pure Platinum case is found by the expression 4.7 where  $A_{Pt}$  is the activity of pure Platinum:

$$\Delta U = \left( \frac{k_B T}{e} \right) \ln \left( \frac{A}{A_{Pt}} \right) \quad (3.7)$$

The HEA found via optimization  $\text{Cu}_t\text{Co}_u\text{Ni}_x\text{Zn}_y\text{Fe}_z$  will then be said as the best fit catalyst for HER.

## **CHAPTER 5: CONCLUSION**

The Hydrogen Evolution Reaction is employed in fuel cells using very expensive Platinum electrocatalysts. They provide very sluggish kinetics due to poor stability and overpotential. It is very important to build highly active and cheaper catalyst options.

It is very important for finding non-noble-transition-metal-based (Ni, Fe, Co, Zn, Cu, etc.) catalysts which show comparable activities to those of benchmarking Pt-based materials. After performing detailed analysis, we can explore cheaper alternative options such as the HEAs CuCoNiZnFe as catalysts for Hydrogen Evolution Reaction.

These alternatives to Platinum based materials will make the hydrogen evolution reaction feasible for the research of alternative fuels replacing the conventional fossil fuels.

## **6. REFERENCES**

1. Ma, R., Lin, G., Zhou, Y. *et al.* A review of oxygen reduction mechanisms for metal-free carbon-based electrocatalysts. *npj Comput Mater*, **2019**,5, 78.
2. Nørskov, J.K., Abild-Pedersen, F., Studt, F., and Bligaard, T. Density functional theory in surface chemistry and catalysis. *Proc. Natl. Acad. Sci. USA*, **2011**, 108, 937–943.
3. Batchelor, T. A. A., Pedersen, J. K., Winther, S. H., Castelli, I. H., Jacobsen, K. W., Rossmeisl, J. High-Entropy Alloys as a Discovery Platform for Electrocatalysis. *Joule*, **2019**, 3, 834-845.
4. Hammer, B., and Nørskov, J.K. Electronic factors determining the reactivity of metal surfaces. *Surf. Sci.*, **1995**, 343, 211–220.
5. Calle-Vallejo, F., Martí'nez, J.I., Garcí'a-Lastra, J.M., Sautet, P., and Loffreda, D. Fast prediction of adsorption properties for platinum nano-catalysts with generalized 503 coordination numbers. *Angew. Chem. Int. Ed.*, **2014**, 53, 8316–8319.
6. Ma, X., and Xin, H. Orbital-wise coordination number for predicting adsorption properties of metal nano-catalysts. *Phys. Rev. Lett.*, **2017**,118, 036101.
7. Tran, K., and Ulissi, Z.W. Active learning across inter-metallics to guide discovery of electrocatalysts for CO<sub>2</sub> reduction and H<sub>2</sub> evolution. *Nat. Catalysis*, **2018**, 1, 696–703.
8. Ma, X., Li, Z., Achenie, L.E.K., and Xin, H. (2015). Machine-learning-augmented chemisorption model for CO<sub>2</sub> electroreduction catalyst screening. *J. Phys. Chem. Lett.*, **2015**, 6, 3528–3533.
9. Hammer, B.; Hansen, L. B.; Nørskov, J. K. Improved Adsorption Energetics Within Density-Functional Theory Using Revised Perdew-Burke-Ernzerhof Functionals. *Phys. Rev. B* **1999**, 59, 7413–7421.

10. Larsen, A. H.; Mortensen, J. J.; Blomqvist, J.; Castelli, I. E.; Christensen, R.; Dułak, M.; Friis, J.; Groves, M. N.; Hammer, B.; Hargus, C.; Hermes, E. D.; Jennings, P. C.; Jensen, P. B.; Kermode, J.; Kitchin, J. R.; Kolsbjerg, E. L.; Kubal, J.; Kaasbjerg, K.; Lysgaard, S.; Maronsson, J. B.; Maxson, T.; Olsen, T.; Pastewka, L.; Peterson, A.; Rostgaard, C.; Schiøtz, J.; Schütt, O.; Strange, M.; Thygesen, K. S.; Vegge, T.; Vilhelmsen, L.; Walter, M.; Zeng, Z.; Jacobsen, K. W. The Atomic Simulation Environment-A Python library for Working with Atoms. *J. Phys.: Condens. Matter* **2017**, *29*, 273002.
11. Mortensen, J. J.; Hansen, L. B.; Jacobsen, K. W. Real-Space Grid Implementation of the Projector Augmented Wave Method. *Phys. Rev. B* **2005**, *71*, No. 035109.
12. Enkovaara, J.; Rostgaard, C.; Mortensen, J. J.; Chen, J.; Dułak, M.; Ferrighi, L.; Gavnholt, J.; Glinsvad, C.; Haikola, V.; Hansen, H. A.; Kristoffersen, H. H.; Kuisma, M.; Larsen, A. H.; Lehtovaara, L.; Ljungberg, M.; Lopez-Acevedo, O.; Moses, P. G.; Ojanen, J.; Olsen, T.; Petzold, V.; Romero, N. A.; Stausholm-Møller, J.; Strange, M.; Tritsarlis, G. A.; Vanin, M.; Walter, M.; Hammer, B.; Häkkinen, H.; Madsen, G. K. H.; Nieminen, R. M.; Nørskov, J. K.; Puska, M.; Rantala, T. T.; Schiøtz, J.; Thygesen, K. S.; Jacobsen, K. W. Electronic Structure Calculations with GPAW: a Real-Space Implementation of the Projector Augmented-Wave Method. *J. Phys.: Condens. Matter* **2010**, *22*, 253202.
13. Gao, Q. S.; Zhang, W. B.; Shi, Z. P.; Yang, L. C.; Tang, Y. Structural Design and Electronic Modulation of Transition-Metal-Carbide Electrocatalysts toward Efficient Hydrogen Evolution. *Adv. Mater.* **2019**, *31*, 1802880.
14. Gileadi, E. Physical Electrochemistry: Fundamentals, Techniques and Applications; Wiley-VCH Verlag GmbH & Co.: Weinheim, **2011**.
15. Paul, S. Hydrogenation and Dehydrogenation by Catalysis. *Berichte der Deutschen Chemischen Gesellschaft* **1911**, *44*, 17.

16. Jaramillo, T. F.; Jørgensen, K. P.; Bonde, J.; Nielsen, J. H.; Horch, S.; Chorkendorff, I. Identification of Active Edge Sites for Electrochemical H<sub>2</sub> Evolution from MoS<sub>2</sub> Nanocatalysts. *Science* **2007**, *317*, 100–102.
17. Parsons, R. The Rate of Electrolytic Hydrogen Evolution and the Heat of Adsorption of Hydrogen. *Trans. Faraday Soc.* **1958**, *54*, 1053–1063.
18. Nørskov, J. K.; Bligaard, T.; Logadottir, A.; Kitchin, J. R.; Chen, J. G.; Pandelov, S.; Nørskov, J. K. Trends in the Exchange Current for Hydrogen Evolution. *J. Electrochem. Soc.* **2005**, *152*, J23–J26.
19. Conway, B. E.; Tilak, B. V. Interfacial Processes Involving Electrocatalytic Evolution and Oxidation of H<sub>2</sub>, and the Role of Chemisorbed H. *Electrochim. Acta* **2002**, *47*, 3571–3594.
20. Trasatti, S. Work Function, Electronegativity, and Electrochemical Behaviour of Metals: III. Electrolytic Hydrogen Evolution in Acid Solutions. *J. Electroanal. Chem. Interfacial Electrochem.* **1972**, *39*, 163–184.
21. Greeley, J.; Nørskov, J. K.; Kibler, L. A.; El-Aziz, A. M.; Kolb, D. M. Hydrogen Evolution Over Bimetallic Systems: Understanding the Trends. *ChemPhysChem* **2006**, *7*, 1032–1035.
22. Seh, Z. W.; Kibsgaard, J.; Dickens, C. F.; Chorkendorff, I.; Nørskov, J. K.; Jaramillo, T. F. Combining Theory and Experiment in Electrocatalysis: Insights into Materials Design. *Science* **2017**, *355*, 4998.
23. Chen, X., Si, C., Gao, Y., Frenzel, J., Sun, J., Eggeler, G., and Zhang, Z. Multicomponent nanoporous platinum–ruthenium–copper–osmium–iridium alloy with enhanced electrocatalytic activity towards methanol oxidation and oxygen reduction. *J. Power Sources* **2015**, *273*, 324–332.
24. Wang, W.R., Wang, W.L., Wang, S.C., Tsai, Y.C., Lai, C.H., and Yeh, J.W. (2012). Effects of Al addition on the microstructure and mechanical property of Al<sub>x</sub>CoCrFeNi high-entropy alloys. *Intermetallics* **2012**, *26*, 44–51.

25. Zhang, Y., Zhou, Y., Lin, J., Chen, G., and Liaw, P. (2008). Solid-solution phase formation rules for multi-component alloys. *Adv. Eng. Mater.* **2008**, *10*, 534–538.
26. Yang, X., and Zhang, Y. (2012). Prediction of high-entropy stabilized solid-solution in multicomponent alloys. *Mater. Chem. Phys.* **2012**, *132*, 233–238.
27. Mizutani, U. (2010). Hume-Rothery Rules for Structurally Complex Alloy Phases (CRC Press) **2010**.
28. Denton, A.R., and Ashcroft, N.W. (1991). Vegard's law. *Phys. Rev. A* **1991**, *43*, 3161–3164.
29. Frydendal, R., Paoli, E.A., Chorkendorff, I., Rossmeisl, J., and Stephens, I.E.L. (2015). Toward an active and stable catalyst for oxygen evolution in acidic media: Ti-stabilized MnO<sub>2</sub>. *Adv. Energy Mater.* **2015**, *5*, 1500991.
30. Calle-Vallejo, F., Tymoczko, J., Colic, V., Vu, Q.H., Pohl, M.D., Morgenstern, K., Loffreda, D., Sautet, P., Schuhmann, W., and Bandarenka, A.S. (2015). Finding optimal surface sites on heterogeneous catalysts by counting nearest neighbors. *Science* **2015**, *350*, 185–189.
31. Abu-Mostafa, Y.S., Magdon-Ismail, M., and Lin, H.-T. (2012). Learning from Data: A Short Course (AMLBook) **2012**, pp. 84–87.
32. Kraft, D. (1988). A Software Package for Sequential Quadratic Programming, Tech. Rep. (DFVLR-FB) **1988**, pp. 18–28.
33. Rossmeisl, J., Karlberg, G.S., Jaramillo, T., and Nørskov, J.K. (2008). Steady state oxygen reduction and cyclic voltammetry. *Faraday Discuss.* **2008**, *140*, 337–346.
34. Stephens, I.E.L., Bondarenko, A.S., Grønbjerg, U., Rossmeisl, J., and Chorkendorff, I. (2012). Understanding the electrocatalysis of oxygen reduction on platinum and its alloys. *Energy Environ. Sci.* **2012**, *5*, 6744–6762.

35. Fischer, J.M., Mahlberg, D., Roman, T., and Groß, A. (2016). Water adsorption on bimetallic PtRu/Pt(111) surface alloys. *Proc. Math. Phys. Eng. Sci.* **2016**, 472, 20160618.
36. Hodgson, A., and Haq, S. (2009). Water adsorption and the wetting of metal surfaces. *Surf. Sci. Rep.* **2009**, 64, 381–451.
37. Vignola, E., Steinmann, S.N., Le Mapihan, K., Vandegehuchte, B.D., Curulla, D., and Sautet, P. (2018). Acetylene adsorption on Pd–Ag alloys: Evidence for limited island formation and strong reverse segregation from Monte Carlo simulations. *J. Phys. Chem. C* **2018**, 122, 15456–15463.
38. Bunce, N.J., and Bejan, D. (2011). Mechanism of electrochemical oxidation of ammonia. *Electrochim. Acta* **2011**, 56, 8085–8093.
39. de Mishima, B.A.L., Lescano, D., Holgado, T.M., and Mishima, H.T. (1998). Electrochemical oxidation of ammonia in alkaline solutions: Its application to an amperometric sensor. *Electrochim. Acta* **1998**, 43, 395–404.